Numerical Investigation of the Middle Atlantic Bight Shelfbreak Frontal Circulation Using a High-Resolution Ocean Hindcast Model

KE CHEN AND RUOYING HE

Department of Marine, Earth and Atmospheric Sciences, North Carolina State University, Raleigh, North Carolina

(Manuscript received 31 March 2009, in final form 12 December 2009)

ABSTRACT

A nested high-resolution ocean model is used to hindcast the Middle Atlantic Bight (MAB) shelfbreak circulation from December 2003 to June 2008. The model is driven by tidal harmonics, realistic atmospheric forcing, and dynamically consistent initial and open boundary conditions obtained from a large-scale circulation model. Simulated shelfbreak sea levels and tracer fields compare favorably with satellite observations and available in situ hydrographic climatology, demonstrating the utility of this nested ocean model for resolving the MAB shelfbreak circulation. The resulting time and space continuous hindcast solutions between January 2004 and December 2007 are used to describe the mean structures and temporal variations of the shelfbreak front and jet, the bottom boundary layer detachment, and the migration of the shelfbreak front. It is found that the shelfbreak jet and boundary convergence reach their maximum intensities in the spring, at which time the foot of the front also migrates to its farthest offshore position. Vorticity analyses reveal that the magnitude ratio of the mean relative vorticity between the seaward and the shoreward portions of the shelfbreak front is about 2:1. The shelfbreak ageostrophic circulation is largely controlled by the viscosity in the boundary layers and by the nonlinear advection in the flow interior. Simulated three-dimensional velocity and tracer fields are used to estimate the transport and heat and salt fluxes across the 200-m isobath. Within the model domain, the total cross-shelf water transport, the total eddy heat flux, and the total eddy salt flux are 0.035 ± 0.26 Sv ($1\ \text{Sv} \equiv 10^6\ \text{m}^3\ \text{s}^{-1}$), $1.0 \times 10^3 \pm 4 \times 10^4$ W m^{-2}, and $6.7 \times 10^{-5} \pm 7.0 \times 10^{-4}$ kg m^{-2} s^{-1}. The empirical orthogonal function (EOF) analysis on the 4-yr shelfbreak circulation hindcast solutions identifies two dominant modes. The first EOF mode accounts for 61% variance, confirming that the shelfbreak jet is a persistent year-round circulation feature. The second mode accounts for 13% variance, representing the baroclinic eddy passages across the shelf break.

1. Introduction

The shelfbreak front in the Middle Atlantic Bight (MAB) is the water mass boundary between the cold freshwater on the MAB shelf and the warm saline water of the slope sea. Associated with the front is a narrow shelfbreak jet, which has been estimated to transport approximately 0.2–0.3 Sv ($1\ \text{Sv} \equiv 10^6\ \text{m}^3\ \text{s}^{-1}$) of water equatorward south of New England (Linder and Gawarkiewicz 1998). This shelfbreak frontal jet is a part of the large-scale buoyancy-driven coastal current system that originates from the Labrador Sea (Chapman and Beardsley 1989; Loder et al. 1998). It exerts strong influence on the coastal environment in the northwest Atlantic, impacting cross-shelf exchanges of mass, heat, and salt; the dispersion of coastal contaminants; and the nutrient supply to coastal ecosystems. For example, the shelfbreak front and jet are found to be important for many commercial fisheries because of the enhanced primary productivity associated with the front (e.g., Marra et al. 1982, 1990; Ryan et al. 1999a,b).

Understanding the shelfbreak frontal dynamics has been the major topic of numerous earlier studies. Hydrographic surveys by Beardsley and Flagg (1976) and Burrage and Garvine (1988) provided synoptic snapshots that generally describe the thermocline structure of the front. Long-term mooring arrays, such as the Nantucket Shoals Flux Experiment (NSFE; Beardsley et al. 1985), the Shelf Edge Exchange Process (SEEP) experiment (Aikman et al. 1988; Houghton et al. 1988) and SEEP II experiment (Houghton et al. 1994; Flagg

Corresponding author address: Dr. Ruoying He, Department of Marine, Earth and Atmospheric Sciences, North Carolina State University, Raleigh, NC 27695.
E-mail: rhe@ncsu.edu

DOI: 10.1175/2009JPO4262.1

et al. 1994) addressed the long-term statistics of the velocity and temperature structure of the front. By area-averaging long-term hydrographic data, Linder and Gawarkiewicz (1998) offered climatological mean conditions of MAB shelfbreak frontal structures, the migration of the front bottom foot, and the associated geostrophic velocity fields. More recently, Fratantoni et al. (2001) studied the structure of shelfbreak jet based on 2-yr (1995–97) ADCP surveys. Although these results provide many valuable insights on the shelfbreak frontal dynamics, they are still limited by temporal and spatial resolutions and are subjected to the question of how representative they are in describing the shelfbreak circulation dynamics. In particular, work including Garvine et al. (1988), Lozier et al. (2002), and Gawarkiewicz et al. (2004) showed that frontal instabilities and shelf–slope interactions are reoccurring features with fine temporal and spatial scales as small as 1–2 days and 8–15 km, respectively. Improved understanding of the MAB shelfbreak circulation and better quantification of its variations therefore require high-resolution space and time continuous realizations of ocean state variables, from which detailed dynamics can be gleaned.

In this study, we approach this problem through a realistic circulation hindcast experiment. We will examine whether a high-resolution nested circulation model, driven by a complete suite of forcing functions, can reproduce known features of the MAB shelfbreak circulation. Unless the model gets the mean states of shelfbreak circulation correct, it is questionable that one can use the model to exam the high-frequency variability associated with the shelfbreak frontal circulation.

We start in section 2 with a description of the shelfbreak ocean model utilized in this research. Section 3 presents model–data comparisons, the structures of simulated mean shelfbreak front and jet, and their temporal variations. More in-depth dynamical analysis and cross-shelf transport and flux estimates are presented in section 4, followed by the discussion and summary in section 5.

2. Model

Our high-resolution shelfbreak simulation was performed with the Regional Ocean Modeling System (ROMS), a free surface, hydrostatic, primitive equation model. ROMS employs split-explicit separation of fast barotropic and slow baroclinic modes, and is formulated in vertically stretched terrain-following coordinates using algorithms described in details by Shchepetkin and McWilliams (2005). The ROMS computational kernel includes high-order advection and time-stepping schemes, weighted temporal averaging of the barotropic mode to reduce aliasing into the slow baroclinic motions, and conservative parabolic splines for vertical discretization. A redefinition of the barotropic pressure-gradient term is also applied in ROMS to reduce the pressure-gradient truncation error, which has previously limited the accuracy of terrain-following coordinate models (Shchepetkin and McWilliams 2005).

The model domain encompasses the shelfbreak region offshore of Nantucket shoals in the northeast and Hudson Canyon in the southwest (Fig. 1). Within the domain, the water depth ranges from 30 to 3000 m. The model's horizontal resolution is 1 km. Vertically, there are 36 terrain-following levels in the water column with higher resolution near the surface and bottom to better resolve ocean boundary layers. The minimum (maximum) model vertical spacing is 0.8 m (211 m) in the boundary layer (the mid water column).

a. Open boundary and initial conditions

To specify open boundary conditions for this shelfbreak model, we nested it inside the Middle Atlantic Bight and Gulf of Maine (MABGOM) ROMS described and validated by He and Chen (2009, manuscript submitted to *J. Geophys. Res.*, hereafter HC). The MABGOM model itself was nested in the global circulation simulation provided by Hybrid Coordinate Ocean Model together with NRL Coupled Ocean Data Assimilation scheme (HyCOM/NCODA; Chassignet et al. 2006). A one-way nesting approach was adopted in this setup to connect the ''parent model'' (MABGOM ROMS) with the ''child model'' (shelfbreak ROMS). Specifically, open boundary conditions (OBCs) were applied to tracers and baroclinic velocity following the method of Marchesiello et al. (2001), whereby Orlanski-type radiation conditions were used in conjunction with relaxation (with time scale of 0.5 days on inflow and 10 days on outflow) to MABGOM solutions. Free surface and depth-averaged velocity boundary conditions were specified using the method of Flather (1976) with the external subtidal values defined by MABGOM ROMS, plus M_2 tidal harmonics from an Advanced Circulation Model for Oceanic, Coastal and Estuarine Waters (ADCIRC) tidal simulation of the western Atlantic (Luettich et al. 1992). The latter M_2 information provides needed tidal mixing, which is an important element of the regional circulation (He and Wilkin 2006). We applied the method of Mellor and Yamada (1982) to compute vertical turbulent mixing, as well as the quadratic drag formulation for the bottom friction specification. Major advantages of this nesting configuration include the following: 1) it allows the child model to incorporate the upstream and deep-ocean forcing in a dynamically consistent and quantitatively accurate manner and 2) the higher resolution enables the shelfbreak ROMS to better resolve the frontal circulation dynamics underpinned in this research.

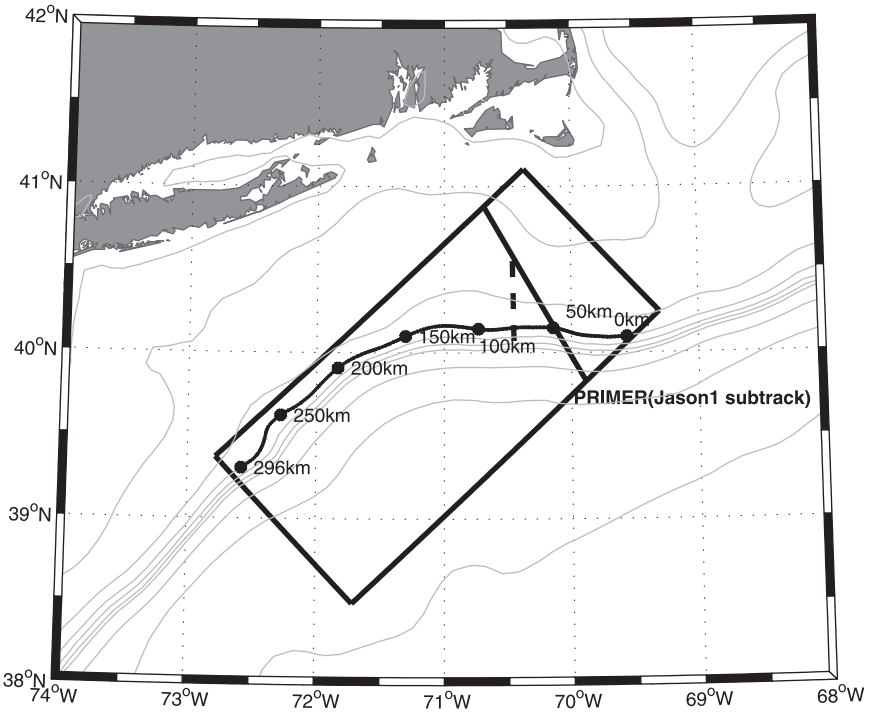

FIG. 1. The high-resolution shelfbreak model domain (box) and the location of Nantucket transect discussed in the paper (dashed line). The satellite track (solid line), along which the SSHA data were sampled. The curve and dots along the 200-m isobath and their associated numbers indicate the along-isobath distance downstream from the model's northeastern boundary.

b. Surface forcing

We utilized surface forcing from National Oceanic and Atmospheric Administration (NOAA) National Centers for Environmental Prediction (NCEP) North America Regional Reanalysis (NARR), which has the spatial and temporal resolutions of 35-km and 3 hourly, respectively. Air–sea fluxes of momentum and buoyancy were computed by applying the standard bulk formulas (Fairall et al. 2003) to NARR marine boundary layer winds, air temperature, relative humidity, air pressure, and ROMS-generated surface current. To further constrain the spatial pattern of the net surface heat flux, we implemented a thermal relaxation term following He and Weisberg (2002) such that

$$K_H \frac{\partial T}{\partial Z} = \frac{Q}{\rho C_p} + c(T_{\text{obs}} - T_{\text{mod}}), \qquad (1)$$

where K_H is the vertical eddy diffusivity, Q is the net surface heat flux, ρ and C_p are the water density and specific heat capacity, $c = 0.5\ \text{day}^{-1}$, and T_{obs} is the daily blended cloud-free surface temperature field generated by NOAA Coast Watch.

The shelfbreak ROMS hindcast ran continuously from December 2003 through January 2008. Initial conditions were taken from the MABGOM ROMS simulation on 1 December 2003.

3. Results

Standard circulation state variables (sea level, currents, temperature, and salinity) were archived at the daily interval. For model validations and analyses described later, we concentrated on the simulation over the period from 1 January 2004 to 31 December 2007. Limited by scarce shelfbreak in situ observations, we used satellite observations and hydrographic climatology to gauge the model's performance.

a. Model data comparisons

1) SEA SURFACE HEIGHT COMPARISON

Satellite altimeter data provide a useful means to examine the model's skill in reproducing sea surface height distribution. For the model validation purpose, we obtained 1/3° × 1/3° along-track SSHA product from French group Archiving, Validation, and Interpretation of Satellite Oceanographic data (AVISO; Rio and Hernadez 2004). There are three satellite tracks inside our shelfbreak model domain. Among them, we focus on a cross-shelf

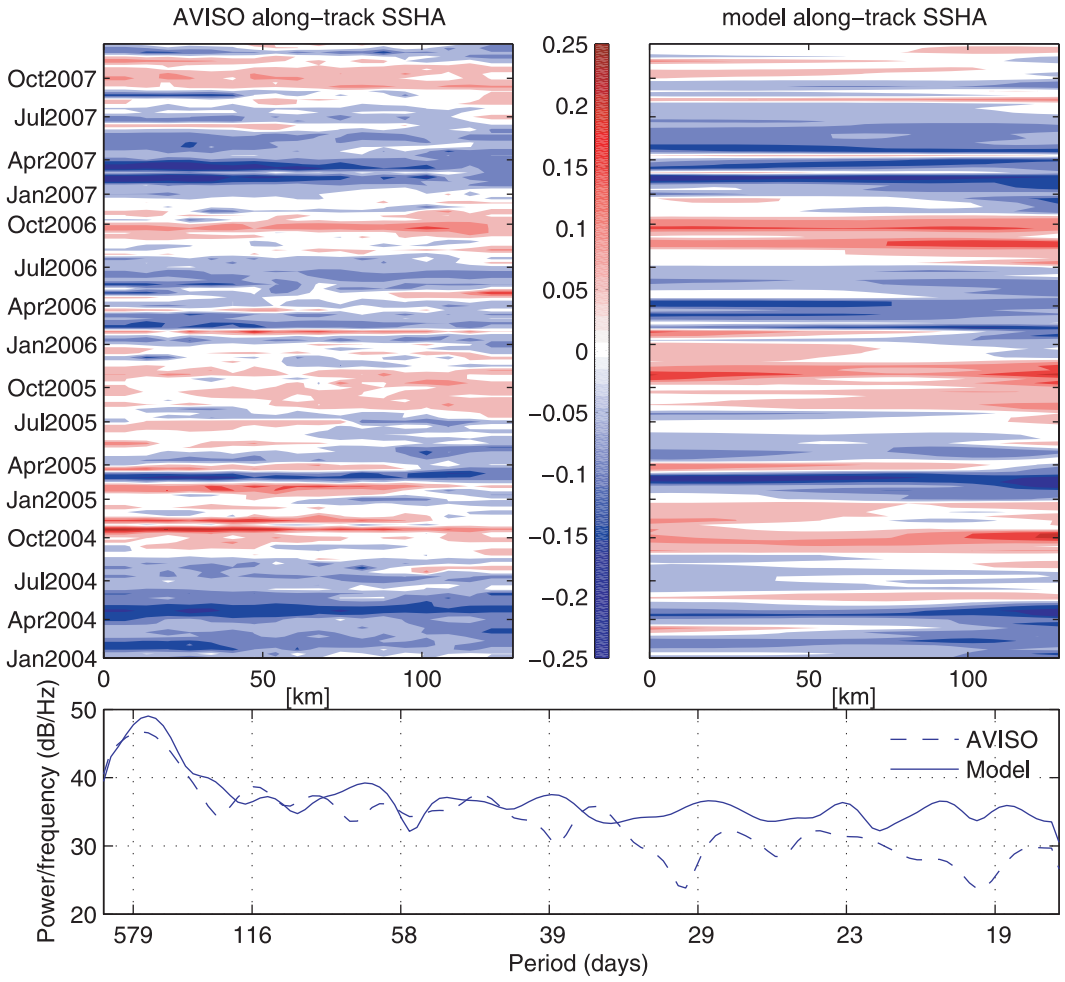

FIG. 2. (top) Hovmöller diagrams of satellite-observed and model-simulated SSHA along the cross-shelf transect for the period from January 2004 to December 2007 and (bottom) the comparison of spectra of satellite-observed (dashed line) and model-simulated (solid line) SSHA in the MAB shelfbreak region.

track that is nearly aligned with the earlier PRIMER section (Fratantoni et al. 2001). Because of that, the along-track satellite data are only available every 9 days; we sampled our simulated subtidal sea surface height anomaly (SSHA) at the same time when altimeter observations were available.

The Hovmöller diagram of observed SSHA shows the sea levels along this cross-shelf transect are the highest (lowest) during the fall (spring) season (Fig. 2, top). The observed absolute surface height variation is up to 0.25 m, which is a result of the combined effects of surface heating and horizontal advection. Such sea level responses were generally reproduced by the shelfbreak model. Although the model is missing some of the fine-scale sea level structures, it captures the seasonal and interannual variability reasonably well. Statistically, the overall correlation coefficient between simulated and observed SSHA is 0.53 with the 95% confidence level. The spectra comparison (Fig. 2, bottom) shows that the model reproduces observed annual cycle and other high-frequency variations. We note that, because the altimeter data are only available every 9 days, some high-frequency variability relevant to the MAB shelfbreak circulation is either aliased or not resolvable by satellite altimeter.

2) SHELFBREAK HYDROGRAPHY COMPARISON

We next sampled the mean temperature and salinity along the Nantucket transect (see Fig. 1) and compared them with early climatology averaged by Linder and Gawarkiewicz (1998) for the similar segment of the MAB shelf break. The Nantucket transect is nearly perpendicular to the local isobath, so the choice of this transect also allows us to directly examine the shelfbreak jet and its along-shelf transport. To be consistent with the Linder and Gawarkiewicz climatology, simulated bimonthly

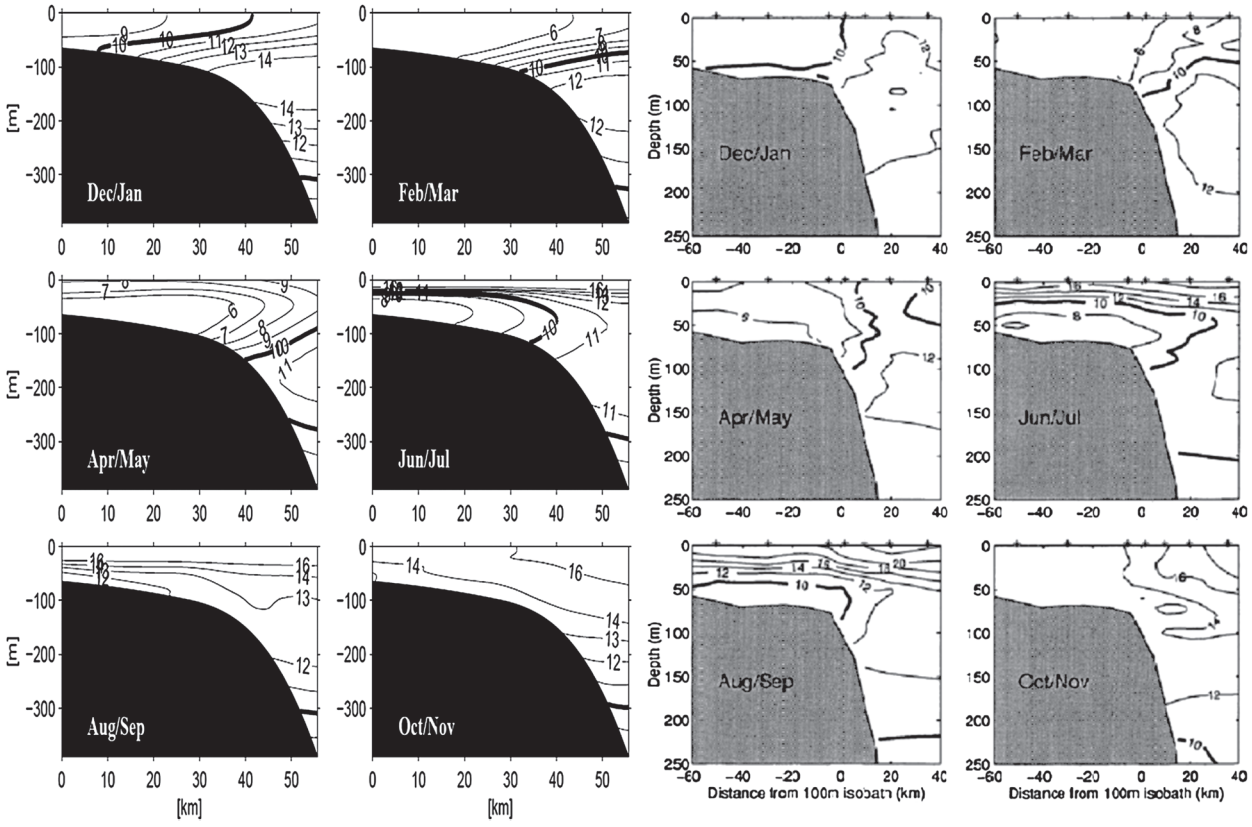

FIG. 3. The bimonthly mean temperature transect comparison between (left two columns) the model solutions and (right) the climatology of Linder and Gawarkiewicz (1998) for (top) Dec–Jan and Feb–Mar, (middle) Apr–May and Jun–Jul, and (bottom) Aug–Sep and Oct–Nov.

mean temperature and salinity fields were averaged based on the 4-yr hindcast solutions.

The bimonthly mean temperature fields (Fig. 3) exhibit strong seasonal variability. During winter months (December–March), surface cooling together with enhanced mixing by convective overturning and storm events keep shelf waters weakly stratified. The thermocline starts to develop as the season progresses. By the spring to summertime (April–July), a strong thermocline has established, separating the warm upper layer from the cold bottom water. The latter becomes the so-called MAB cold pool described by Beardsley and Flagg (1976) and Houghton et al. (1982), among other studies. Further offshore, both observation and simulation show an abrupt horizontal temperature gradient at the shelf break, known as the ''shelfbreak front.'' In fall (August–November), the shelf waters transition from vertically stratified to horizontally stratified. As a result, the shelfbreak temperature front becomes less pronounced by this time compared to its spring and summer conditions. The bimonthly salinity fields (Fig. 4) exhibit relatively weaker seasonal variability. Unlike the temperature, both the simulation and observation show the shelfbreak salinity front is a persistent feature throughout the year, with a gradient of 1–2 psu difference over 10–20 km. We note the simulated mean temperature and salinity fields reported here are based on the 4-yr shelfbreak hindcast, whereas the Linder and Gawarkiewicz climatology was produced by a time and space averaging of hydrographic data collected in the vicinity of MAB shelf break over nearly 100 yr. Despite differences in the time span and the temporal and spatial resolutions between the two, it is encouraging to see that the regional shelfbreak model is capable of reproducing essential features of shelfbreak temperature and salinity and their respective seasonal evolutions. These general agreements verify the utility of the model, lending confidence for using its hindcast solutions to study the shelfbreak circulation dynamics.

3) DECORRELATION-SCALE COMPARISON

Based on ship observations in July 1996, Gawarkiewicz et al. (2004) provided a set of decorrelation-scale estimations for the MAB shelfbreak circulation. Although our model hindcast period did not include the year of 1996, we calculated the decorrelation scale using simulated circulation fields in July 2006 and made comparisons with

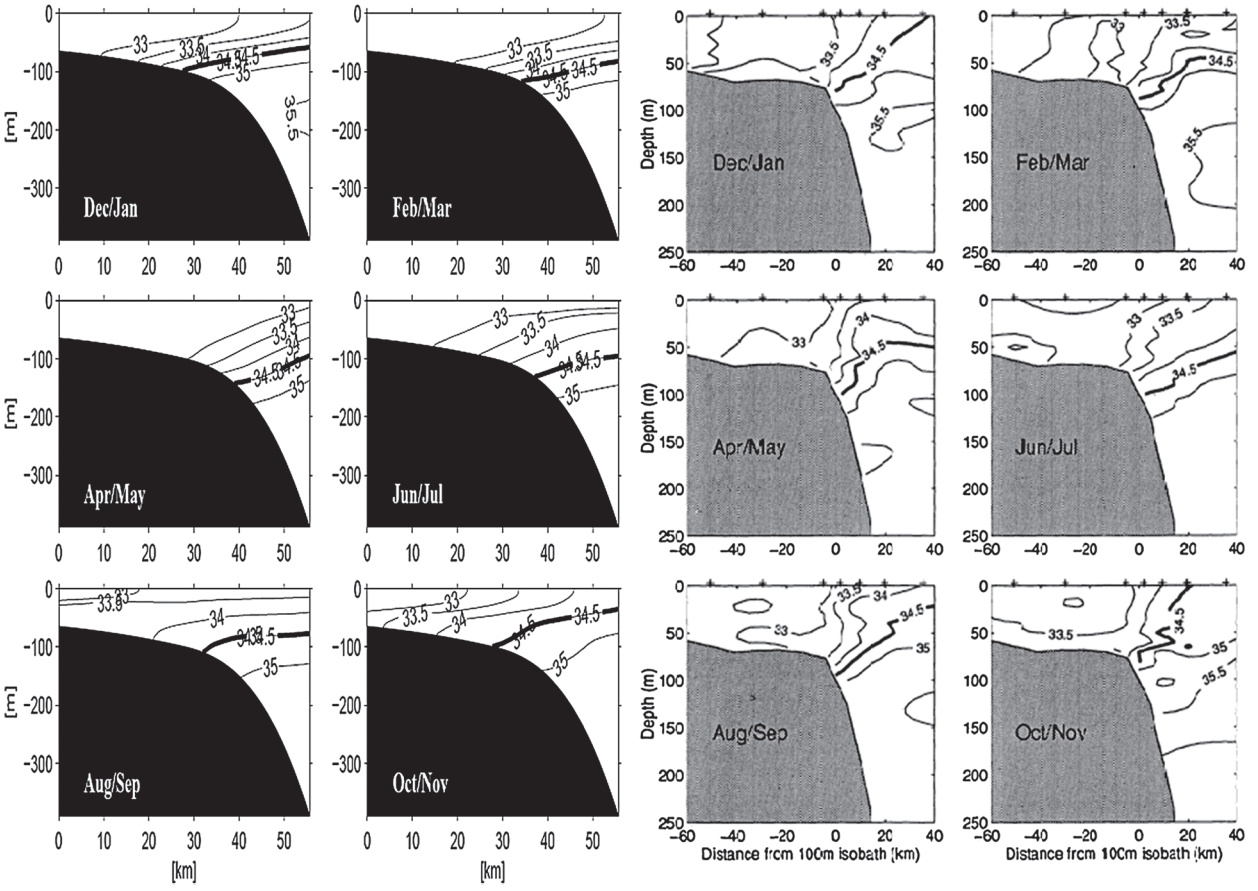

FIG. 4. As in Fig.3, but for salinity transects.

their observational counterparts (Table 1). Depending on the state variable being examined, the observation-based analysis shows the decorrelation scale varies from 7 to 20 km. Our model based analyses are consistently larger (varying from 12 to 22 km) than those inferred from observations but certainly in the comparable ranges. The shelfbreak circulation fields in July 1996 and July 2006 would be quite different, but the intrinsic dynamic scales of the system are expected to be similar. The general agreement between the observed and simulated scales suggests the shelfbreak ROMS can indeed capture the essential features of the MAB shelfbreak circulation.

b. Model analysis

We next use the high-resolution space and time continuous hindcast solutions to characterize the MAB shelfbreak jet and frontal structures along the Nantucket transect.

1) MEAN SHELFBREAK FRONTAL STRUCTURES

First we concentrated on the structures of mean temperature, salinity, and along- and across-shelf velocity fields (Fig. 5), each obtained by temporally averaging their respective solutions from 1 January 2004 to 31 December 2007. The mean temperature field highlights the coexistence of the cold pool on the shelf and the temperature front at the shelf break. Within the cold pool area, the bottom water is about 4°–5°C cooler than the surface water. At the shelf break, the upward titled temperature front extends from the bottom to 20 m below the surface. A similar shelfbreak frontal structure is also seen in the mean salinity field. However, the salinity front extends all the way to the surface, presenting a clearer surface signature than the temperature front does.

The mean alongshore velocity transect shows the shelfbreak circulation consists of an equatorward shelfbreak jet and a near-bottom poleward current, a structure consistent with the finding of Flagg et al. (2006). Further examinations (not shown) indicate this near-bottom flow reversal is a local feature that can be explained by the thermal wind balance described by Chapman and Lentz (1994). In the summer, however, this locally generated flow mergers with the poleward slope current, resulting in an enhanced northward transport in the Slope Sea.

TABLE 1. Comparisons of state variable decorrelation scales derived from in situ survey in July 1996 (Gawarkiewicz et al. 2004) and from the shelfbreak model hindcast results in July 2006.

Variable (at ~54 m)	Obs (July 1996) (km)	Model (July 2006) (km)
Temperature	7	12
Salinity	7–8	12
Density	20	16
u component velocity	11–12	22
v component velocity	12	20

The shelfbreak jet moves at 0.1 m s^{-1}, with the majority of its flow trapped within the upper 70 m. Consistent with findings of earlier studies (Gawarkiewicz et al. 2004; Fratantoni et al. 2001), the jet core is located at the shoreward side of the shelfbreak front. The *e*-folding scales are 50 m and 30 km for the shelf-jet depth and width, respectively. The resulting along-jet transport is 0.42 Sv, a value comparable with previous estimates (Beardsley et al. 1985; Linder and Gawarkiewicz 1998; Fratantoni et al. 2001). The cross-shelf mean velocity exhibits a layered structure similar to what was discussed by Lentz (2008). It has a seaward-moving surface flow (the upper 25 m) and a shoreward-moving interior flow, which is underlaid by another weak seaward-moving flow near the bottom. It should be noted that the 4-yr temporal averaging may smooth out small-scale frontal structures that may otherwise be observed in the synoptic in situ surveys. We will examine the small-scale variability in detail in a future correspondence.

2) BIMONTHLY MEAN SHELFBREAK JET STRUCTURES

To quantify the temporal variations of the shelfbreak jet associated with the bimonthly hydrography presented in section 3a, we computed bimonthly velocity means (Fig. 6). In December and January, the shelfbreak jet is surface trapped within a thin (<50 m) but broad (>20 km) upper layer. The poleward slope current is largely absent at this time of the year. Consequently, the equatorward shelfbreak currents transport a volume of 0.72 Sv to the south, the largest value throughout the year. The shelfbreak jet then weakens in February and March, with the core of the jet shifting offshore. This is accompanied by an onshore motion of the slope current. Transports of theses two currents counteract each other, resulting in a net equatorward transport of only 64% of its winter value. In April–May, the shelfbreak

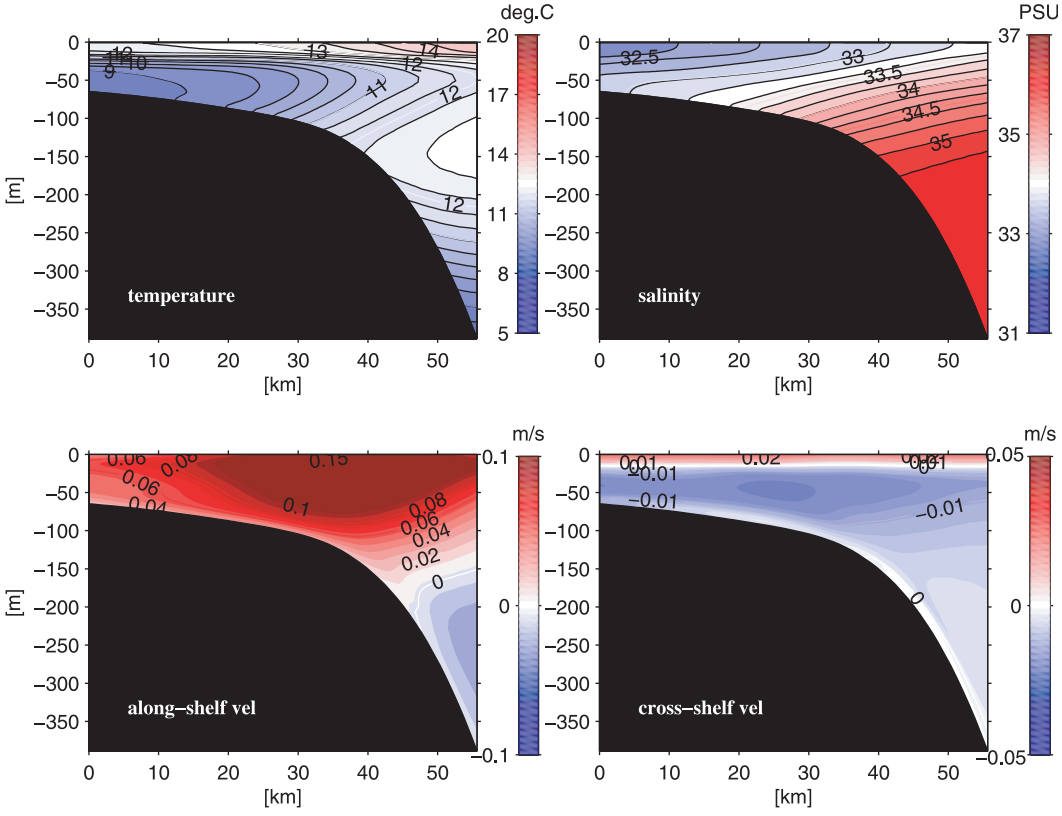

FIG. 5. Model-simulated mean (top left) temperature, (top right) salinity, (bottom left) along-shelf velocity, and (bottom right) cross-shelf velocity fields along the Nantucket transect.

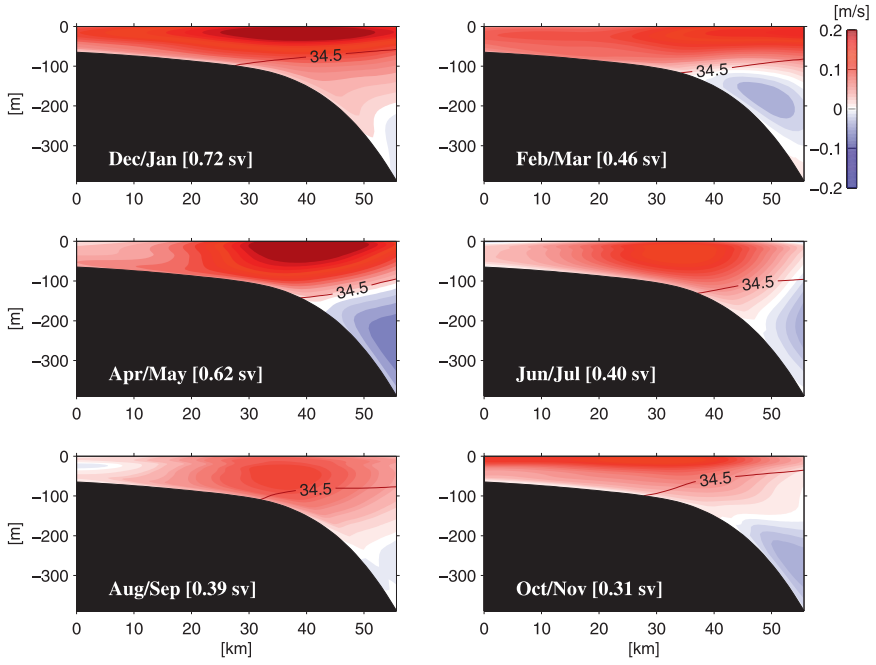

FIG. 6. Simulated bimonthly mean along-shelf velocity fields and their associated net equatorward transport. The black contour lines are the 34.5 isohaline of the respective bimonthly salinity field to indicate the location of shelfbreak front.

jet gets stronger with the core of jet confined to within a few kilometers shoreward of the shelf break. The jet speed reaches its annual maximum, 0.3 m s^{-1}, a value that is consistent with the observation of Fratantoni et al. (2001). The slope current seaward of the shelf break is similarly intensified but to a lesser extent. Consequently, the net equatorward transport is 0.62 Sv, the second highest value of the year. Starting in June/July, the jet begins to weaken with its core moving onshore and deepening. The maximum velocity now decreases to 0.1 m s^{-1}. These changes are in response to shelf water destratification associated with enhanced cooling and mixing, leading to a weakened across-shelf density gradient (e.g., Fig. 3). By October and November, the shelfbreak jet structure is less clear. Counteracted by the enhanced poleward slope current, the net equatorward transport now reaches its minimum value of the year.

3) BIMONTHLY MEAN BBL DETACHMENT

An important feature of the MAB shelfbreak circulation is the convergent flow near the bottom of the shelfbreak front and its related bottom boundary layer (BBL) detachment process (Gawarkiewicz and Chapman 1992; Chapman and Lentz 1994; Barth et al. 1998; Pickart 2000; Linder et al. 2004). Pickart (2000) showed a useful means to quantify such BBL detachment is through the accumulated property change (APC) calculation. The basic idea is that upwelling along the isopycnal layer in which the detachment is occurring should result in a weaker water property gradient. Hence, by computing the accumulated theta change (ATC) along tilted isopycnals in a cross-front transect and tracking tongues of low ATC, one can asses the intensity of bottom boundary layer detachment. Following this idea, we computed water density and its associated ATC using bimonthly temperature and salinity fields. The resulting bimonthly shelfbreak ATC fields (Fig. 7) indicate that bottom convergence is indeed a discernable feature in the winter, spring, and summer seasons with its intensity proportional to the degree of isopycnal titling. That is, larger BBL convergences are observed when the isopycnals are more steeply tiled at the shelf break.

No significant ATC tongue structure is identified in the fall when isopycnals are relatively flat, suggesting a shutdown of the BBL convergence. We note that findings here are consistent with Linder et al. (2004) BBL discussion. One caveat is that the present ATC calculations are based on the bimonthly mean tracer fields. A more rigorous quantification of the BBL detachment and shelfbreak upwelling rate estimation would require a more focused case study using instantaneous three-dimensional tracer and circulation fields. This is an ongoing effort that we will report in a future correspondence.

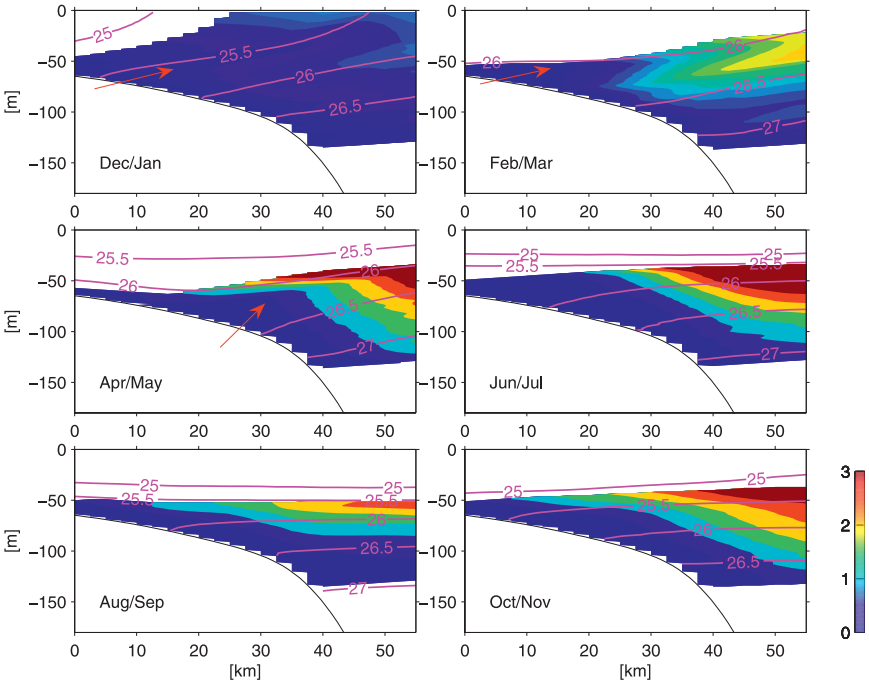

FIG. 7. Bimonthly accumulated theta change (ATC) fields along the Nantucket transect. The ATC calculation is based on modeled bimonthly density fields. The purple lines are the isopycnals, and the color shading stands for the intensity of ATC. The upward-tilted, low-value ATC (indicated by arrows) is an indication of the BBL convergence and detachment.

4) CROSS-SHELF MIGRATION OF SHELFBREAK FRONT

Following Beardsley and Flagg (1976) and Linder and Gawarkiewicz (1998), we investigated spatial variations of the foot of the front, using the 34.5 isohaline to define the front boundary (Fig. 8, left). In general, the 34.5 isohaline tilts upward. Consistent with our earlier discussion, the largest titling angle occurs in the spring season, when the maximum speed of baroclinic shelfbreak jet occurs. Throughout the year, the monthly-mean foot position migrates between 100- and 160-m isobaths, which translates into a horizontal displacement of 15 $\sim$ 20 km. In terms of the water depth of the frontal foot, the monthly position histogram (Fig. 8, right) indicates that the front moves to its farthest onshore position in the winter (November and December) and its farthest offshore position in the spring (April and May), respectively. Consistent with finding of Linder and Gawarkiewicz (1998), results here suggest that in situ samplings of the shelf break front would require a sufficient spatial coverage to resolve variations of the front. Although the seasonal excursions of 15 $\sim$ 20 km is roughly the same order of magnitude as the width of shelfbreak jet, the front still remains close to the shelf break. Chapman (2000) shows the front does not adjust much differently to the presence or absence of the shelfbreak topography. The mechanisms for such a frontal trapping remain to be better understood.

4. Discussion

a. *Vorticity and momentum balance*

Based on the mean shelfbreak circulation fields, we can compute the relative vorticity (ζ) $(\partial v/\partial x) - (\partial u/\partial x)$ along the Nantucket transect (Fig. 9, left). The resulting mean vorticity field, scaled by the local Coriolis parameter, gives the Rossby number $R_o = \zeta/f$. Seaward of the shelfbreak jet R_o is positive with a maximum value of 0.15. Shoreward of the jet, R_o is negative with a value approaching -0.07. The result here compares favorably with the observational-based vorticity calculation reported by Fratantoni et al. (2001; Fig. 9, right). It is also in agreement with Gawarkiewicz et al. (2001), showing that the absolute ratio of relative vorticity is about 2:1 between the seaward and the shoreward portions of the front. A further investigation on the relative vorticity in fixed coordinates indicates that the $\partial v/\partial x$ and $-\partial u/\partial y$ terms each account for nearly 50% of the relative vorticity. On synoptic scales (not shown), the relative vorticity of the simulated jet shows a very wide range, varying from $-0.78f$ to $2.3f$. Examinations of the mean shelfbreak circulation (Fig. 5) indicate the presence of

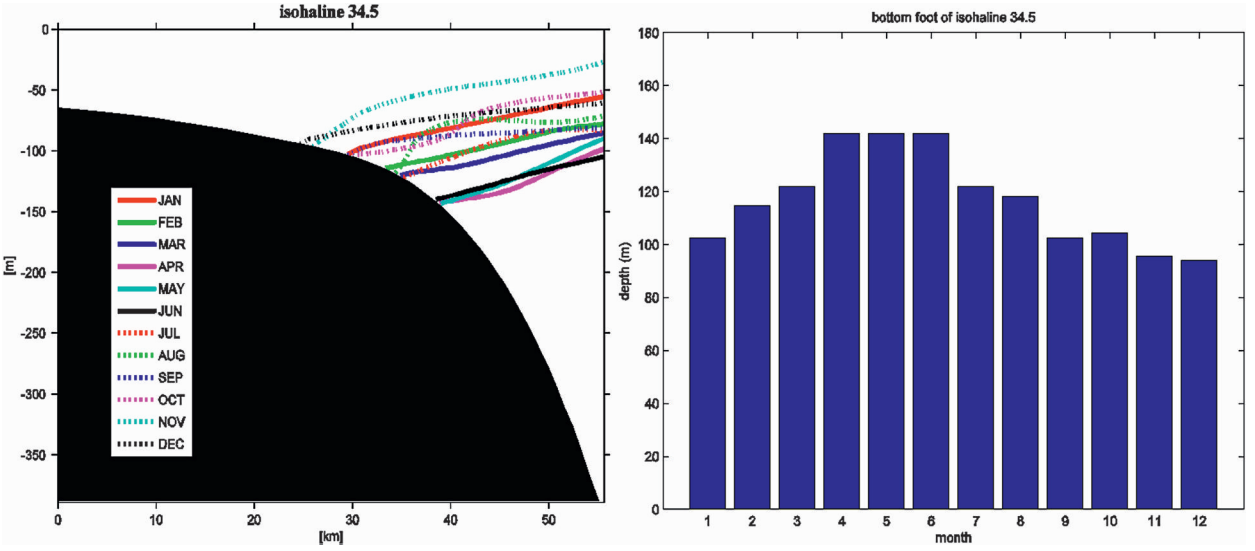

FIG. 8. (left) Monthly migrations of the shelfbreak frontal foot and (right) the histogram showing the corresponding depth of the frontal foot in each month.

poleward slope current induces a large velocity shear, contributing to a stronger cyclonic circulation seaward of the shelf break. The consistency between observed and simulated vorticity fields further confirms that the shelfbreak model captures the essence of shelfbreak circulation dynamics.

Term-by-term momentum analysis offers additional insights on the shelfbreak circulation. By examining the relative importance of the local rate of change, the Coriolis force, the horizontal pressure-gradient force (PGF), horizontal and vertical advection terms, and the horizontal and vertical viscosity terms, one can identify key balances dominating the shelfbreak circulation structure. We focus on the mean momentum balance in the cross-shelf direction (Fig. 10). As expected, both the Coriolis force and pressure-gradient force are the leading (an order of magnitude larger than others) terms, and together they constitute the geostrophic balance. Indeed, the shelfbreak jet and the poleward-moving slope current are to the first order geostrophic flows. The residual of Coriolis force plus pressure-gradient force leads to the ageostrophic circulation. The ageostrophic momentum is balanced largely by the frictional viscosity in the surface and bottom boundary layers. The residual of those two is further balanced by the nonlinear advection presented primarily in the flow interior. The sum of ageostrophic momentum, viscosity, and advection terms gives rise to the local rate of change of the mean across-shelf velocity (last panel in Fig. 10), which is four orders of magnitudes smaller than the Coriolis force. In reality, we expect the local rate of change of the shelfbreak circulation at any given time to be a significantly large number because of the transitory nature of the system (e.g., Lozier et al. 2002). Therefore, a large number of snapshots would have to be ensembled to produce a steady-state mean field. The fact that the simulated local rate of change term is very small suggests that the temporal averaging of 4 yr of daily model output fields produces a credible representation of the mean state of the shelfbreak circulation.

b. *Cross-shelf transport and flux*

Quantifying the slope/shelf water mass and flux exchanges has been a long-standing research problem in the MAB (Beardsley and Boicourt 1981; Loder et al. 1998; Lozier and Gawarkiewicz 2001; Fratantoni et al. 2001; Gawarkiewicz et al. 2004). Here, we approach this problem by using simulated circulation fields. To do that, we followed HC by selecting the 200-m isobath as the shelf–slope boundary and compute the cross-shelf water mass transport. Simulated three-dimensional velocity fields were first rotated into normal and tangential components relative to the local orientations of the 200-m isobath. The resulting normal component of velocity U_N was then integrated with local depth Z and along-isobath length S to yield the volume transport value according to

$$Q = \int_0^{s_o} \int_{-H}^{\eta} u_N(s, z)\, ds\, dz, \qquad (2)$$

where s_o is the along-isobath distance. This calculation reveals that, across the 200-m isobath within the shelfbreak model domain, the total transport is 0.035 ± 0.26 Sv. It is worth noting that the standard deviation of such transport is an order of magnitude larger than

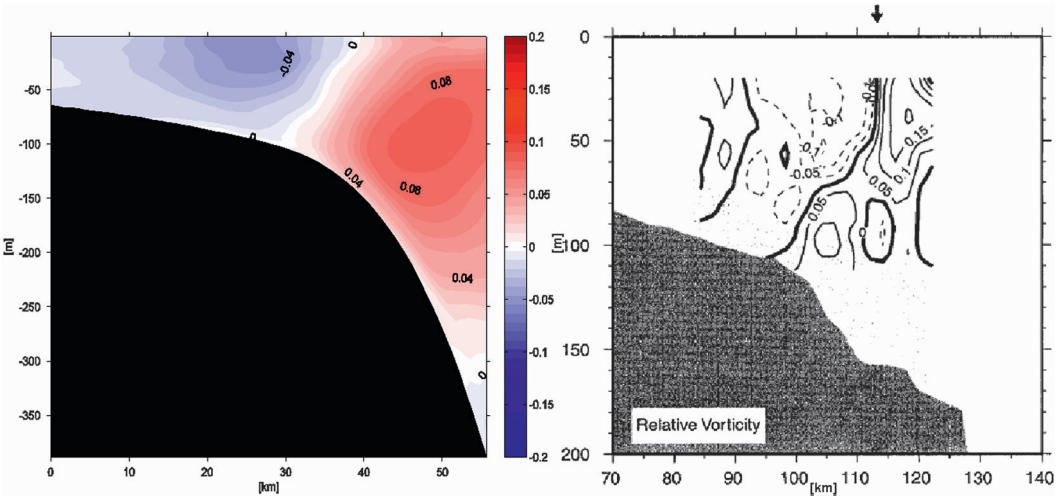

FIG. 9. The comparison between (left) simulated and (right) observed (adopted from Fratantoni et al. 2001) mean vorticity fields at the shelf break. Both fields are scaled by the local Coriolis parameter.

the mean, indicating that across-shelfbreak mass exchange is highly variable. We also note that the meander of the jet can induce large fluctuations in the cross-shelf transport. Thus it is prudent to state that the value above does not necessarily imply the net shelf–deep-ocean exchange.

The spatial distribution of such variability is examined in Fig. 11. In general, the mean transport near the Nantucket Shoal (0–100 km along isobath) is weakly onshore. Immediately downstream (100–200 km), the mean transport becomes weakly offshore with a value of ~0.002 Sv. The overall variations over these two segments are both relatively small. Fluctuations in the transport values become larger approaching Hudson Canyon off New York (200–300 km). Here, the standard deviations range from −0.02 to 0.02 Sv, which are likely related to topographic steering by abrupt bathymetric changes and eddy activities often observed in this area.

The cross-shelf eddy flux of any quantity Φ can be estimated by the method proposed by Garvine et al. (1989) such that

$$F(z) = \frac{1}{\Delta z \Delta x} \int_{z-(\Delta z/2)}^{z+(\Delta z/2)} \int_{x_1}^{x_2} \Phi(x, z_1)\, dx\, dz_1. \qquad (3)$$

For the heat flux, we defined

$$\Phi = \rho C_p (T - T_m)(v - v_m). \qquad (4)$$

For the salt flux, we defined

$$\Phi = \frac{\rho}{1000} (S - S_m)(v - v_m), \qquad (5)$$

where ρ is water density; C_p is the seawater specific heat; and S, T, and v are the salinity, temperature, and cross-shelf velocity, respectively. The variables with subscript m indicate the temporal mean values along the 200-m isobath within the shelfbreak model domain.

We found the 4-yr mean eddy heat flux is shoreward at $1.0 \times 10^3 \pm 1.4 \times 10^4$ W m^{-2}, indicating on average that the slope sea is acting as the source of heat for the shelf waters. Depending on the local and deep-ocean forcing conditions, individual monthly eddy heat flux ranges from 4.8×10^4 W m^{-2} (shoreward) in May 2004 to -3.0×10^4 W m^{-2} (seaward) in October 2004. Further investigations into the seasonal trend of the total cross-shelf eddy heat flux (not shown) indicate that the heat flux tends to be onshore during the winter and spring seasons and offshore during summer and fall seasons.

The mean eddy salt flux is found to be shoreward at $6.7 \times 10^{-5} \pm 7.0 \times 10^{-4}$ kg m^{-2} s^{-1}. Over the 4 yr, the largest onshore flux (0.0026 kg m^{-2} s^{-1}) occurred in May 2004, and the largest offshore flux (−0.0011 kg m^{-2} s^{-1}) occurred in October 2004. This model-based mean salt flux value is consistent with Gawarkiewicz et al. (2004) with regards to its onshore transport direction. However, the magnitude is one to two orders of magnitude smaller than earlier observational estimates (e.g., Gawarkiewicz et al. 2004; Garvine et al. 1989), which were based on either single point measurement or some limited ship transects for a short time period. Aside from the temporal averaging in our flux calculation that may have smoothed the variability, differences in sampling locations and durations between the simulation and observations also contribute to the magnitude difference.

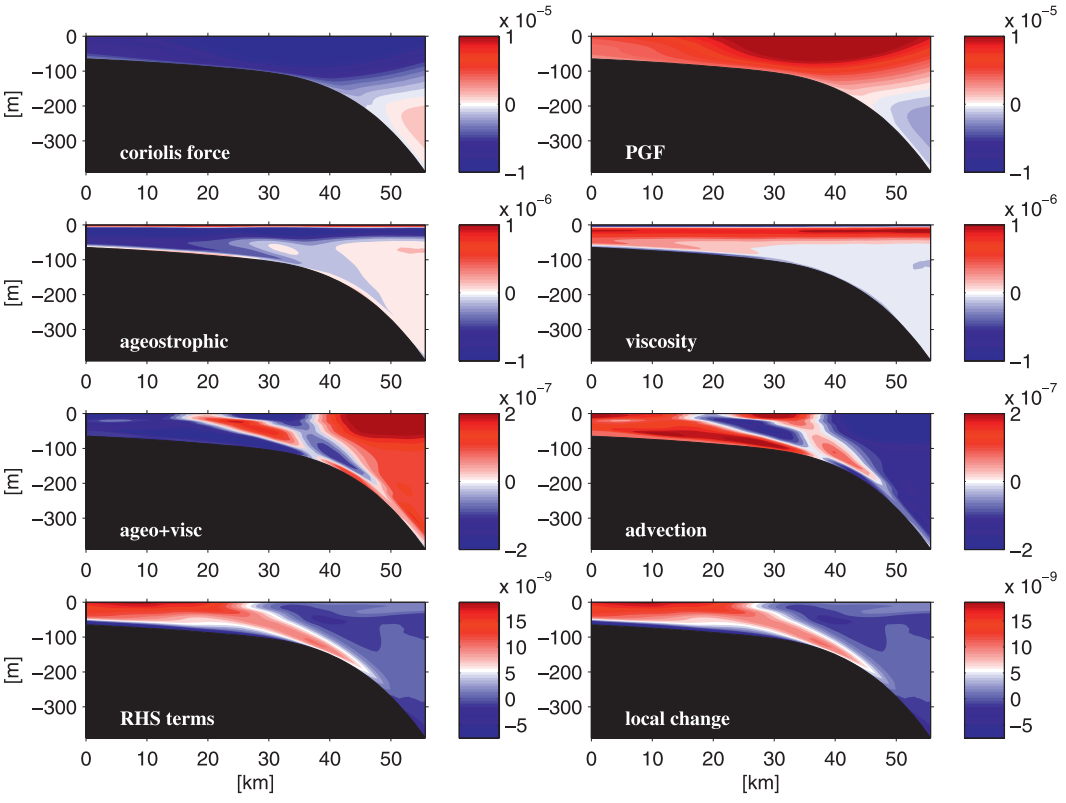

FIG. 10. The mean cross-shelf momentum balance: From top to bottom and left to right, the Coriolis force, the PGF, the residual of Coriolis plus PGF terms (i.e., ageostrophic term), the viscosity term, the residual of ageostrophic term plus viscosity, the nonlinear advection term, the residual of ageostrophic plus viscosity and advection terms, and the local rate of change term.

c. *Dominant modes of shelfbreak jet*

Although the focus of this study is on the mean state of the MAB shelfbreak frontal circulation, we can assess the dominant modes and temporal variability of the front and jet by applying an empirical orthogonal function (EOF) analysis to the simulated current fields along the Nantucket transect. Because along-shelf and cross-shelf velocity fields are dynamically connected, a bivariant EOF method (He et al. 2005) that concurrently considers both u and v velocity components was adopted. Specifically, the data matrix $\mathbf{A}$ was defined as

$$\mathbf{A} = \begin{pmatrix} u \\ v \end{pmatrix}. \tag{6}$$

The EOF decomposition of $\mathbf{A}$ gives

$$\mathbf{A}(x, z, t) = \sum_{n=1}^{N} a_n(t) F_n(x, z), \tag{7}$$

where a_n and $F_n(x, z)$ are the temporal evolution functions (principal components) and spatial eigenfunctions (EOF) of each mode, respectively.

The first EOF mode accounts for 62% of variance (Fig. 12). As expected, the along-shelf velocity mode highlights the existence of the shelfbreak jet. The jet is located shoreward of the shelf break. It is surface trapped with a characteristic width of about 40–60 km. The spatial mode of the across-shelf velocity again reveals a layered vertical structure, which consists of a shoreward flow in the interior and seaward flows in both surface and bottom boundary layers. The principal component (PC1) of the first EOF mode is almost entirely positive, suggesting the equatorward shelfbreak jet and layer-structured cross-shelf flow patterns are persistent shelfbreak circulation features. PC1 also reveals that some short-duration flow reversals do occur sporadically, which are presumably related to strong atmospheric forcing and frontal instability (Fratantoni and Pickart 2003). Overall, larger PC1 values occur during late winter and spring seasons. Consistent with our early discussion [section 3b(2)], they imply that the shelfbreak jet reaches its maximum intensity during these times.

The second EOF mode accounts for 13% of total variance. Interestingly, this mode displays contrasting flow patterns between the shelf and the slope in along-shelf

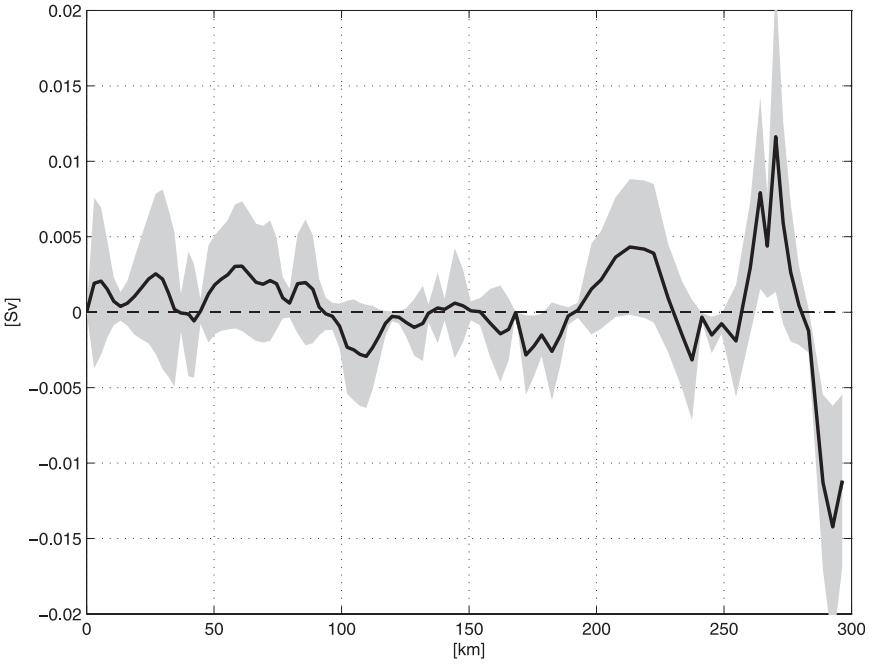

FIG. 11. The cross-shelf volume transport along the 200-m isobath inside the shelfbreak ROMS domain. The x axis is the along-isobath distance starts from 0 (off the Nantucket shoal) to 300 km (off the Hudson Canyon). The solid curve is the mean cross-shelf volume transport over the 4-yr period, and the gray area stands for its standard deviation.

direction. The cross-shelf component is surface intensified and negative throughout the entire water column. The second principal component (PC2) suggests that this mode is associated with significant temporal variability that changes signs of spatial mode. Overall, this mode seems to be related to the baroclinic eddy passages across the shelf break. The positive PC2 indicates cyclonic eddies translating shoreward, whereas the negative PC2 corresponds to anticyclonic eddies translating seaward. Generation of baroclinic eddies are subject to large-scale surface and deep-ocean forcing conditions and the flow interaction with the bottom topography. Although no clear seasonal cycle is found, the frequency spectra calculation (not shown) on the PC2 show the energy peaks around the periods of 70, 160, and 200 days, respectively. With some 25% of the variance remaining in higher modes, a reconstruction of the shelfbreak circulation to account for its high-frequency responses would require several more modes.

5. Summary

A 1-km-resolution regional circulation model was developed to hindcast the MAB shelfbreak circulation from December 2003 to June 2008. The model considered realistic atmospheric and tidal forcing. Its subtidal open boundary conditions were specified via one-way nesting with an existing shelf-wide MABGOM circulation simulation by HC. Hindcast solutions were compared with satellite altimeter data, hydrographic climatology for the MAB shelf break, and observation-based decorrelation-scale estimations. General agreements were found, indicating this shelfbreak circulation model is capable of capturing essential dynamics of the MAB shelfbreak circulation. Because we focused on the mean structures of the shelfbreak current and hydrography in this study, time and space continuous circulation hindcast fields from January 2004 to December 2007 were used to construct the temporal means and bimonthly averages of shelfbreak ocean states.

Our analysis showed that the MAB shelfbreak jet is a year-round surface-intensified flow. On average, it has characteristic width and trapping depth of 60 km and 100 m, respectively, transporting 0.42 Sv equatorward. The jet reaches its maximum speed (0.3 m s^{-1}) in the spring, when the shelfbreak temperature and salinity fronts fully develop. Throughout the year, the bottom foot of the shelfbreak front migrates between 100- and 150-m isobaths, reaching its farthest offshore (onshore) position in April and May (November and December). The accumulated theta change (ATC) calculation within shelfbreak isopycnals suggests the bottom boundary layer detachment is most significant during winter and spring seasons.

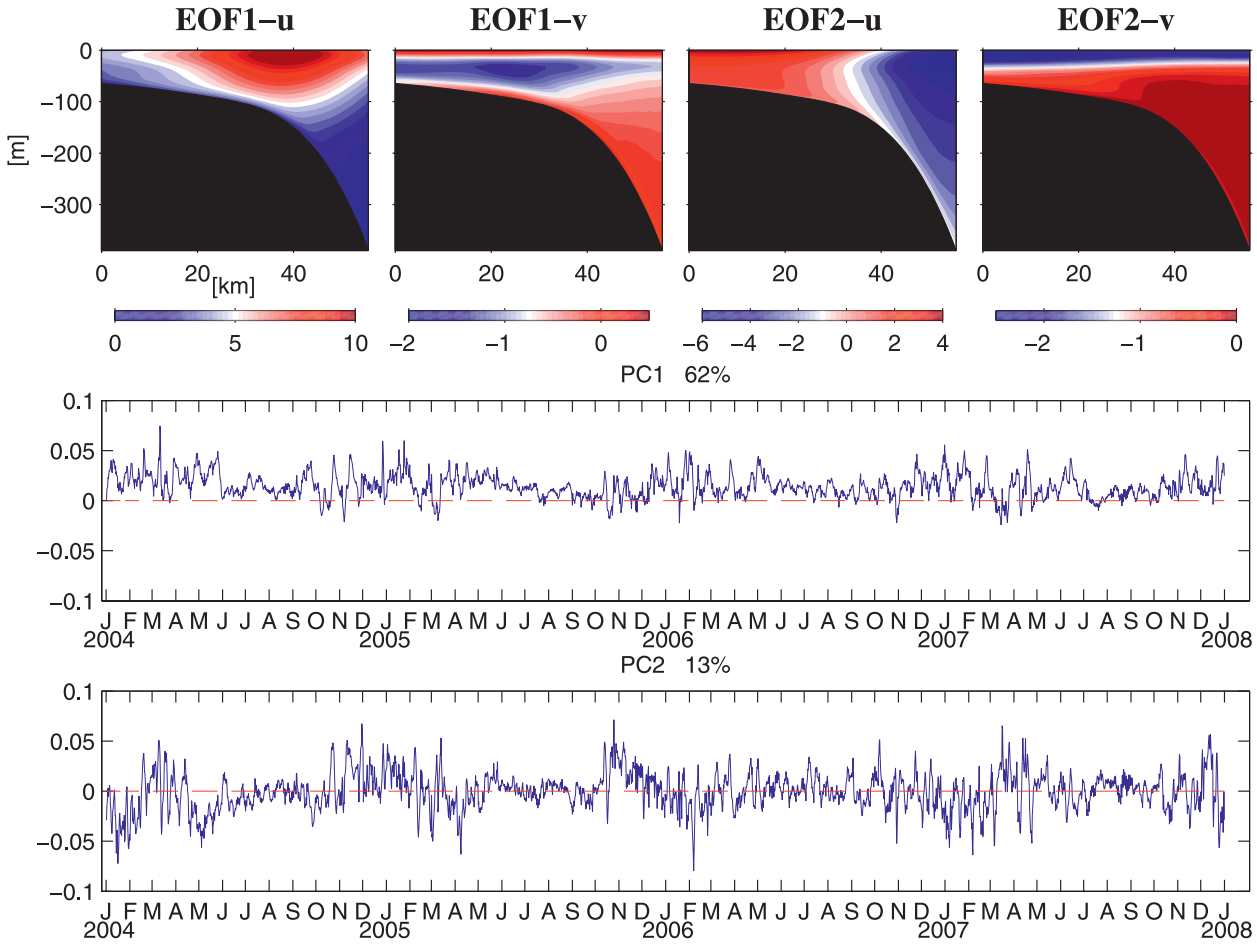

FIG. 12. (top) The first two EOF modes of simulated shelf break circulation, and (middle), (bottom) their corresponding principal components: u (v) is the alongshore (cross shelf) velocity component along the Nantucket transect.

The relative vorticity analysis indicates that the larger velocity shear exists seaward of the shelf break and that the vorticity ratio is roughly 2:1 between the seaward portion and shoreward portion of the shelfbreak current. The geostrophy dominates the momentum balance of the shelfbreak jet. The viscosity in the boundary layers and the nonlinear advection in the interior, play important roles in determining the ageostrophic flow. The cross-shelf volume transport and its associated eddy heat and salt fluxes were estimated along the 200-m isobath within the model domain. These values are characterized by small means with large standard deviations, suggesting the shelf–slope exchanges across the MAB shelf break are highly variable. Indeed, the EOF analysis of the velocity fields along the Nantucket transect indicates that, while the shelfbreak jet is the dominant mode, the structure and intensity of the current are subject to complex interactions betweens stratification, wind forcing, baroclinic instabilities, and eddies. A better understanding of their roles in controlling the shelfbreak circulation dynamics can be further achieved in the future by focusing on synoptic-scale events using the high-resolution shelfbreak model developed here. Clearly, deterministic predictions of the shelfbreak frontal circulation and its associated material property transport between the shelf and deep ocean will also require advanced observational infrastructure together with sophisticated techniques for data assimilation (e.g., He et al. 2005; He and Wilkin 2006). In that regard, the emerging MAB shelfbreak pioneer array, as well as the new in situ observations it is about to collect, would be a great asset.

Acknowledgments. Research support provided through ONR Grant N00014-06-1-0739 and NASA Grant NNX07AF62G are appreciated. We are indebted to G. Gawarkiewicz and D. McGillicuddy for their valuable discussions and suggestions throughout the course of this study. We also thank two anonymous reviewers for their insightful comments and suggestions.

REFERENCES

Aikman, F., III, H. W. Ou, and R. W. Houghton, 1988: Current variability across the New England continental shelf-break and slope. *Cont. Shelf Res.,* **8,** 625–651.

Barth, J. A., D. Bogucki, S. D. Pierce, and P. M. Kosro, 1998: Secondary circulation associated with a shelfbreak front. *Geophys. Res. Lett.,* **25,** 2761–2764.

Beardsley, R. C., and C. N. Flagg, 1976: The water structure, mean currents, and shelf/slope water front on the New England continental shelf. *Mem Soc. Roy. Sci. Liege,* **6,** 209–225.

——, and W. C. Boicourt, 1981: On estuarine and continental-shelf circulation in the Middle Atlantic Bight. *Evolution of Physical Oceanography,* B. A. Warren and C. Wunsch, Eds., MIT Press, 198–233.

——, D. C. Chapman, K. H. Brink, S. R. Ramp, and R. Schlitz, 1985: The Nantucket Shoals Flux Experiment (NSFE79). Part I: A basic description of the current and temperature variability. *J. Phys. Oceanogr.,* **15,** 713–748.

Burrage, D. M., and R. W. Garvine, 1988: Summertime hydrography at the shelfbreak front in the Middle Atlantic Bight. *J. Phys. Oceanogr.,* **18,** 1309–1319.

Chapman, D. C., 2000: Boundary layer control of buoyant coastal currents and the establishment of a shelfbreak front. *J. Phys. Oceanogr.,* **30,** 2941–2955.

——, and R. C. Beardsley, 1989: On the origin of shelf water in the Middle Atlantic Bight. *J. Phys. Oceanogr.,* **19,** 384–391.

——, and S. J. Lentz, 1994: Trapping of a coastal density front by the bottom boundary layer. *J. Phys. Oceanogr.,* **24,** 1464–1479.

Chassignet, E. P., H. E. Hurlburt, O. M. Smedstad, G. R. Halliwell, P. J. Hogan, A. J. Wallcraft, R. Baraille, and R. Bleck, 2006: The HYCOM (Hybrid Coordinate Ocean Model) data assimilative system. *J. Mar. Syst.,* **65,** 60–83.

Fairall, C. W., E. F. Bradley, J. E. Hare, A. A. Garchev, and J. Edson, 2003: Bulk parameterization of air–sea fluxes: Updates and verification for the COARE algorithm. *J. Climate,* **16,** 571–591.

Flagg, C. N., R. W. Houghton, and L. J. Pietrafesa, 1994: Summertime thermocline salinity maximum intrusions in the Middle Atlantic Bight. *Deep-Sea Res. II,* **41,** 325–340.

——, M. Dunn, D.-P. Wang, H. T. Rossby, and R. L. Benway, 2006: A study of the currents of the outer shelf and upper slope from a decade of shipboard ADCP observations in the Middle Atlantic Bight. *J. Geophys. Res.,* **111,** C06003, doi:10.1029/2005JC003116.

Flather, R. A., 1976: A tidal model of the northwest European continental shelf. *Mem. Soc. Roy. Sci. Liege,* **6,** 141–164.

Fratantoni, P. S., and R. S. Pickart, 2003: Variability of the shelf break jet in the Middle Atlantic Bight: Internally or externally forced? *J. Geophys. Res.,* **10,** 3166, doi:10.1029/2002JC001326.

——, ——, D. J. Torres, and A. Scotti, 2001: Mean structure and dynamics of the shelfbreak jet in the Middle Atlantic Bight during fall and winter. *J. Phys. Oceanogr.,* **31,** 2135–2156.

Garvine, R. W., K.-C. Wong, G. G. Gawarkiewicz, R. K. McCarthy, R. W. Houghton, and F. Aikman III, 1988: The morphology of shelf break eddies. *J. Geophys. Res.,* **93,** 15 593–15 607.

——, ——, and ——, 1989: Quantitative properties of shelfbreak eddies. *J. Geophys. Res.,* **94,** 14 475–14 483.

Gawarkiewicz, G. G., and D. C. Chapman, 1992: The role of stratification in the formation and maintenance of shelf-break fronts. *J. Phys. Oceanogr.,* **22,** 753–772.

——, F. Bahr, R. C. Bearsley, and K. H. Brink, 2001: Interaction of a Slope Eddy with the Shelfbreak Front in the Middle Atlantic Bight. *J. Phys. Oceanogr.,* **31,** 2783–2796.

——, K. H. Brink, R. C. Bearsley, M. Caruso, J. F. Lynch, and C. Chiu, 2004: A large-amplitude meander of the shelfbreak front during summer south of New England: Observations from the Shelfbreak PRIMER experiment. *J. Geophys. Res.,* **109,** C03006, doi:10.1029/2002JC001468.

He, R., and R. H. Weisberg, 2002: West Florida shelf circulation and temperature budget for the 1999 spring transition. *Cont. Shelf Res.,* **22,** 719–748.

——, and J. L. Wilkin, 2006: Barotropic tides on the southeast New England shelf: A view from a hybrid data assimilative modeling approach. *J. Geophys. Res.,* **111,** C08002, doi:10.1029/2005JC003254.

——, D. J. McGillicuddy, D. R. Lynch, K. W. Smith, C. A. Stock, and J. P. Manning, 2005: Data assimilative hindcast of the Gulf of Maine coastal circulation. *J. Geophys. Res.,* **110,** C10011, doi:10.1029/2004JC002807.

Houghton, R. W., R. Schlitz, R. C. Beardsley, B. Butman, and J. L. Chamberlin, 1982: The Middle Atlantic Bight cold pool: Evolution of the temperature structure in summer 1979. *J. Phys. Oceanogr.,* **12,** 1019–1029.

——, F. Aikman III, and H. W. Ou, 1988: Shelf-slope water frontal structure, and cross-shelf exchange at the New England shelfbreak. *Cont. Shelf Res.,* **8,** 687–710.

——, C. N. Flagg, and L. J. Pietrafesa, 1994: Shelf-slope water frontal structure, motion, and eddy heat flux in the southern Middle Atlantic Bight. *Deep-Sea Res. II,* **41,** 273–306.

Lentz, S. J., 2008: Observations and a model of the mean circulation over the Middle Atlantic Bight continental shelf. *J. Phys. Oceanogr.,* **38,** 1203–1221.

Linder, C. A., and G. Gawarkiewicz, 1998: A climatology of the shelf break front in the Middle Atlantic Bight. *J. Geophys. Res.,* **103,** 18 405–18 423.

——, ——, and R. S. Pickart, 2004: Seasonal characteristics of bottom boundary layer detachment at the shelfbreak front in the Middle Atlantic Bight. *J. Geophys. Res.,* **109,** C03049, doi:10.1029/2003JC002032.

Loder, J. W., B. Petrie, and G. Gawarkiewicz, 1998: The coastal ocean off northeastern North America: A large-scale view. *The Sea: The Global Coastal Ocean,* Vol. 11, Regional Studies and Syntheses, A. R. Robinson and K. H. Brink, Eds., Wiley, 105–133.

Lozier, M. S., and G. Gawarkiewicz, 2001: Cross-frontal exchange in the Middle Atlantic Bight as evidenced by surface drifters. *J. Phys. Oceanogr.,* **31,** 2498–2510.

——, M. S. C. Reed, and G. G. Gawarkiewicz, 2002: Instability of a shelfbreak front. *J. Phys. Oceanogr.,* **32,** 924–944.

Luettich, R. A., Jr., J. J. Westerink, and N. W. Scheffner, 1992: ADCIRC: An advanced three- dimensional circulation model for shelves, coasts and estuaries, report 1: Theory and methodology of ADCIRC-2DDI and ADCIRC-3DL. U.S. Army Corps of Engineers Tech. Rep. DRP-92-6, 137 pp.

Marchesiello, P., J. C. McWilliams, and A. Shchepetkin, 2001: Open boundary conditions for long-term integration of regional oceanic models. *Ocean Modell.,* **3,** 1–20.

Marra, J., R. W. Houghton, D. C. Boardman, and P. J. Neale, 1982: Variability in surface chlorophyll a at a shelf-break front. *J. Mar. Res.,* **40,** 575–591.

——, ——, and C. Garside, 1990: Phytoplankton growth at the shelfbreak front in the Middle Atlantic Bight. *J. Mar. Res.,* **48,** 851–868.

Mellor, G. L., and T. Yamada, 1982: Development of a turbulence closure model for geophysical fluid problems. *Rev. Geophys.,* **20,** 851–875.

Pickart, R. S., 2000: Bottom boundary layer structure and detachment in the shelfbreak jet of the Middle Atlantic Bight. *J. Phys. Oceanogr.,* **30,** 2668–2686.

Rio, M.-H., and F. Hernadez, 2004: A mean dynamic topography computed over the world ocean from altimetry, in situ measurements, and a geoid model. *J. Geophys. Res.,* **109,** C12032, doi:10.1029/2003JC002226.

Ryan, J. P., J. A. Yoder, J. A. Bath, and P. C. Cornillon, 1999a: Chlorophyll enhancement and mixing associated with meanders of the shelf break front in the Mid-Atlantic Bight. *J. Geophys. Res.,* **104** (C10), 23 479–23 493.

——, ——, and P. C. Cornillon, 1999b: Enhanced chlorophyll at the shelfbreak of the Mid-Atlantic Bight and Georges Bank during the spring transition. *Limnol. Oceanogr.,* **44,** 1–11.

Shchepetkin, A. F., and J. C. McWilliams, 2005: The Regional Oceanic Modeling System (ROMS): A split-explicit, free surface, topography-following-coordinate oceanic model. *Ocean Modell.,* **9,** 347–404.